Magnetic Resonance Imaging 61 (2019) 20–32

Contents lists available at ScienceDirect

Magnetic Resonance Imaging

journal homepage: www.elsevier.com/locate/mri

Original contribution

Multi-shot Echo Planar Imaging for accelerated Cartesian MR Fingerprinting: An alternative to conventional spiral MR Fingerprinting

Arnold Julian Vinoj Benjamin[a,b,*], Pedro A. Gómez[c,d], Mohammad Golbabaee[e], Zaid Bin Mahbub[b], Tim Sprenger[d], Marion I. Menzel[d], Michael Davies[a], Ian Marshall[b]

[a] School of Engineering, Institute for Digital Communications, University of Edinburgh, United Kingdom
[b] Centre for Clinical Brain Sciences, University of Edinburgh, United Kingdom
[c] Computer Science, Technische Universität München, Munich, Germany
[d] GE Global Research, Munich, Germany
[e] Computer Science Department, University of Bath, United Kingdom

ARTICLE INFO

Keywords:
Cartesian MRF
Multi-shot EPI
Quantitative maps

ABSTRACT

Purpose: To develop an accelerated Cartesian MRF implementation using a multi-shot EPI sequence for rapid simultaneous quantification of T1 and T2 parameters.
Methods: The proposed Cartesian MRF method involved the acquisition of highly subsampled MR images using a 16-shot EPI readout. A linearly varying flip angle train was used for rapid, simultaneous T1 and T2 quantification. The results were compared to a conventional spiral MRF implementation. The acquisition time per slice was 8s and this method was validated on two different phantoms and three healthy volunteer brains in vivo.
Results: Joint T1 and T2 estimations using the 16-shot EPI readout are in good agreement with the spiral implementation using the same acquisition parameters (< 4% deviation for T1 and < 6% deviation for T2). The T1 and T2 values also agree with the conventional values previously reported in the literature. The visual qualities of fine brain structures in the multi-parametric maps generated by multi-shot EPI-MRF and Spiral-MRF implementations were comparable.
Conclusion: The multi-shot EPI-MRF method generated accurate quantitative multi-parametric maps similar to conventional Spiral-MRF. This multi-shot approach achieved considerable k-space subsampling and comparatively short TRs in a similar manner to spirals and therefore provides an alternative for performing MRF using an accelerated Cartesian readout; thereby increasing the potential usability of MRF.

1. Introduction

Quantitative MRI (q-MRI) is fast emerging as a clinically useful modality in diagnostic MR imaging because these images provide clinicians additional information that helps in more accurate diagnosis, improved disease monitoring and better treatment planning [1,2,3]. Quantitative parameters like proton density (PD), T1 and T2 relaxation times, etc. vary for normal and abnormal tissues and can give an indication of neurodegenerative disorders in the brain that are not readily detectable from conventional structural MR images [4,5,6]. The estimation of tissue parameters helps in greater tissue discrimination, segmentation and classification to improve disease detection and monitoring. For example, T1 mapping has various applications such as the detection of neurodegenerative disorders like multiple sclerosis (MS) [7], Alzheimer's disease [8], assessment of myocardial infarction [9] and characterizing fiber bundle anatomy in diffusion MRI [10] while T2 mapping is used for applications in ageing and cognitive decline [11], quantification of myocardial edema [12] and evaluation of articular cartilage damage in the knee [13,14]. However, clinical time constraints have prevented the widespread clinical use of parametric mapping techniques [15,16]. Recent emergence of rapid parametric mapping techniques such as Magnetic Resonance Fingerprinting (MRF) [17] and its various extensions [18–20] have shown that it is possible to generate multiple quantitative parametric maps simultaneously in a very short scan duration that is clinically feasible. MRF offers a new approach to simultaneously quantify multiple tissue properties rapidly within a single scan by acquiring the transient-state signal that is sensitive to multiple imaging parameters such as flip angle (FA) and

Abbreviations: MRF, Magnetic Resonance Fingerprinting; EPI, Echo Planar Imaging; TR, repetition time

* Corresponding author at: School of Engineering, Institute for Digital Communications, University of Edinburgh, United Kingdom.
E-mail address: arnold.benjamin@ed.ac.uk (A.J.V. Benjamin).

https://doi.org/10.1016/j.mri.2019.04.014
Received 8 October 2018; Received in revised form 19 April 2019; Accepted 29 April 2019

repetition time (TR). Acquiring a series of subsampled images rapidly while constantly varying imaging parameters leads to spatial and temporal incoherence resulting in characteristic signal evolutions, which depend on the physical properties of the underlying tissue, such as relaxation times. The unique signal evolutions or 'fingerprints' are matched to a precomputed dictionary to generate multi-parametric quantitative maps.

The first MRF implementation was able to simultaneously quantify T1, T2 and off-resonance effects and was based on a balanced steady state free precession (bSSFP) sequence which was sensitive to field inhomogeneities and produced banding artefacts [17]. These effects were mitigated by the use of an unbalanced steady state free precession sequence (SSFP) for multi-parametric quantification [18,21–23]. The most commonly used sampling strategy in MRF is interleaved spiral sampling because it allows considerable subsampling of k-space and also provides more control for efficient traversal of the k-space trajectory [17,18]. Despite its numerous advantages, the spiral sampling scheme has been shown to be susceptible to gradient inaccuracies [24] and high frequency artefacts due to non-sampling of k-space corners [25] and its availability is limited which prevents its widespread use in clinical protocols [26].

Cartesian sampling schemes for MRF primarily based on single-shot Echo Planar Imaging (EPI) that have been proposed are promising but are not a like-for-like comparison with the spiral sampling strategy for MRF [27–31]. Since single-shot EPI implementations do not allow subsampling in a similar manner to the spiral scheme, the entire k-space has to be traversed for every frame during acquisition which results in much longer TRs than would be achievable with spiral sampling. It also places a burden on the gradient performance of the scanner due to the short echo spacing necessary to minimise image distortions in single-shot EPI [32]. Simulation results show that shorter TRs result in better T1 and T2 sensitivity for certain MRF sequences (see Supplementary material).

In this study, a multi-shot EPI-MRF approach is proposed that not only allows considerable k-space subsampling but can also achieve shorter TRs that are comparable to conventional Spiral-MRF implementations in a sufficiently short scan duration. Multi-shot EPI can yield better SNR, reduced blurring and lower ghost intensity while it also reduces the burden on gradients and RF hardware such as gradient amplitude and slew rate compared to single-shot EPI [32,33]. It also has the advantage of reduced distortions due to magnetic field inhomogeneity [34]. Unlike Spiral-MRF, multi-shot EPI-MRF has a solid theoretical basis in terms of compressed sensing theory [35,36].

A multi-shot EPI readout is used in this study to generate accurate T1 and T2 maps and compared with Spiral-MRF. An Iterative Projection Algorithm (IPA) called BLoch matching response recovery through Iterated Projection (BLIP) is used to improve the accuracy of the generated parametric maps [35,36]. Sequence parameters such as RF pulse, Inversion Time, FA train, TR and bandwidth are identical for both EPI-MRF and Spiral-MRF experiments in order to quantitatively assess the conformity of both methods.

2. Methods

2.1. Pulse sequence design

The original MRF paper that was based on a bSSFP sequence was sensitive to banding artefacts [17]. In order to overcome this, Jiang et al. [18] suggested the use of an unbalanced SSFP sequence also sometimes called FISP sequence. In the multi-shot EPI-MRF method introduced here, we also used an unbalanced SSFP sequence but we made the following changes compared to previous papers:

(i) a variable flip angle ramp instead of a pseudorandom FA schedule was used to improve the T1 and T2 quantification efficiency in fewer number of repetitions (N) [23] than the original FISP-MRF sequence [18]. Fig. 1 shows the T1-T2 sensitivity of exemplary values of grey matter (GM), white matter (WM) and cerebrospinal fluid (CSF) at 3T that were simulated for the unbalanced SSFP sequence using the Extended Phase Graph (EPG) model for two different FA schedules, namely: a) Linear Ramp FA Pattern from 1° to 70° with N = 500 repetitions and b) Pseudorandom FA pattern with N = 1000 repetitions that was used by Jiang et al. [18].

The sensitivity is defined as the correlation coefficient (i.e. the normalized inner product) measuring the correlation between a query T1-T2 pair within the dictionary and the responses for a range of T1-T2 values. It depends on the shape of the magnetization response and is a function of the flip angle schedule, number of repetitions, TR, Echo Time (TE), Inversion Time (TI) and the readout time. The sensitivity plots are calculated using the same EPG model used to construct the dictionary which is mathematically described in [37,38]. Fig. 1 also shows that by using the Linear Ramp FA pattern, a very similar T1-T2 sensitivity for GM and WM is achieved in only half the number of repetitions and a significantly better T1-T2 sensitivity for CSF can be achieved when compared to the pseudorandom FA pattern. The FA was incremented by (70 - 1) °/500 = 0:138° for every repetition.

(ii) a subsampled Cartesian readout (with readout time 6.976 ms) using 16-shot EPI (see Fig. 2a) was used to eliminate re-gridding, perform faster reconstruction and avoid high frequency artefacts that appeared in spiral readouts due to the non-sampling of k-space corners as shown by Cline et al. [25].

2.2. Sequence parameters

The scanning was performed on a 3T GE MR750w scanner with a 12 channel receive only head RF coil (GE Medical Systems, Milwaukee, WI). The study was approved by the local ethics committee. Both EPI-MRF and Spiral-MRF data were acquired from phantom and healthy volunteer brains using the variable FA ramp that has been described in Section 2.1.

The EPI-MRF acquisition used about 58.72% of the readout time (i.e. 4.096 ms) to collect 8 unique lines of k_y-space data for every shot. A reference scan with the EPI blips turned off was performed for phase correction of EPI raw data. Gradient spoiling of about three and a half cycles was introduced by the spoiler gradient G_z (see Fig. 2a) to make it an unbalanced SSFP acquisition. The zero order gradient moments for G_x and G_y were nulled towards the end of every readout (between 6.464 ms and 6.976 ms) to ensure constant magnetization for each shot throughout the acquisition (see Fig. 2b).

A variable density spiral trajectory with 89 interleaves was used to collect Spiral-MRF data. Each interleave was rotated by a golden-ratio angle (i.e. 111.246°). The duration of spiral readout was 4.096 ms. No reference measurements were made for the spiral trajectory.

The minimum achievable TR for EPI (i.e. 16 ms) was used for both EPI-MRF and Spiral-MRF acquisitions for fair comparison even though the TR could be further reduced for Spiral-MRF. Both acquisitions had bandwidth (BW) = 250 kHz, Field of View (FOV) = 22.5 × 22.5 cm2, 128 × 128 matrix size and 5 mm slice thickness. A global inversion pulse with TI = 18 ms was used at the beginning of the acquisition to increase the T1 sensitivity of the sequence. The TE was 2 ms and 3.488 ms respectively for the spiral and EPI acquisitions. TE is defined as the time at which the centre of k-space is sampled and is assumed to be constant for every shot (approximately half the readout time). The acquisition time for a single slice was 8 s.

2.3. Phantom scans

16-shot EPI-MRF and Spiral-MRF datasets using a variable FA ramp

[23] were acquired for 500 repetitions from a gel based phantom (Diagnostic Sonar, Livingston, UK) which consisted of 12 tubes, each having different T1 and T2 values. The gels were made from agarose doped with gadolinium which represents an ideal test material for MR imaging studies as gels with any desired T1 and T2 value can be produced by varying the material composition. Reference T1 and T2 values measured under controlled conditions were provided by the manufacturer and were used for comparison with the multi-parametric values estimated by the two MRF methods (i.e. EPI-MRF and Spiral- MRF).

2.3.1. Gold standard T1 and T2 spin echo measurements

The T1 and T2 values of the phantom were characterized by using the gold standard Inversion Recovery Spin Echo sequence for T1 estimation and single echo spin echo method (SE) for T2 estimation. These values were compared to the T1 and T2 values estimated by EPI-MRF and Spiral-MRF.

The T1 values of the different tubes in the phantom were measured by the IR-SE sequence with 32 inversion times ranging from 0.05 s to 4 s, parallel imaging ASSET factor 2, TR of 12 s, a matrix size of

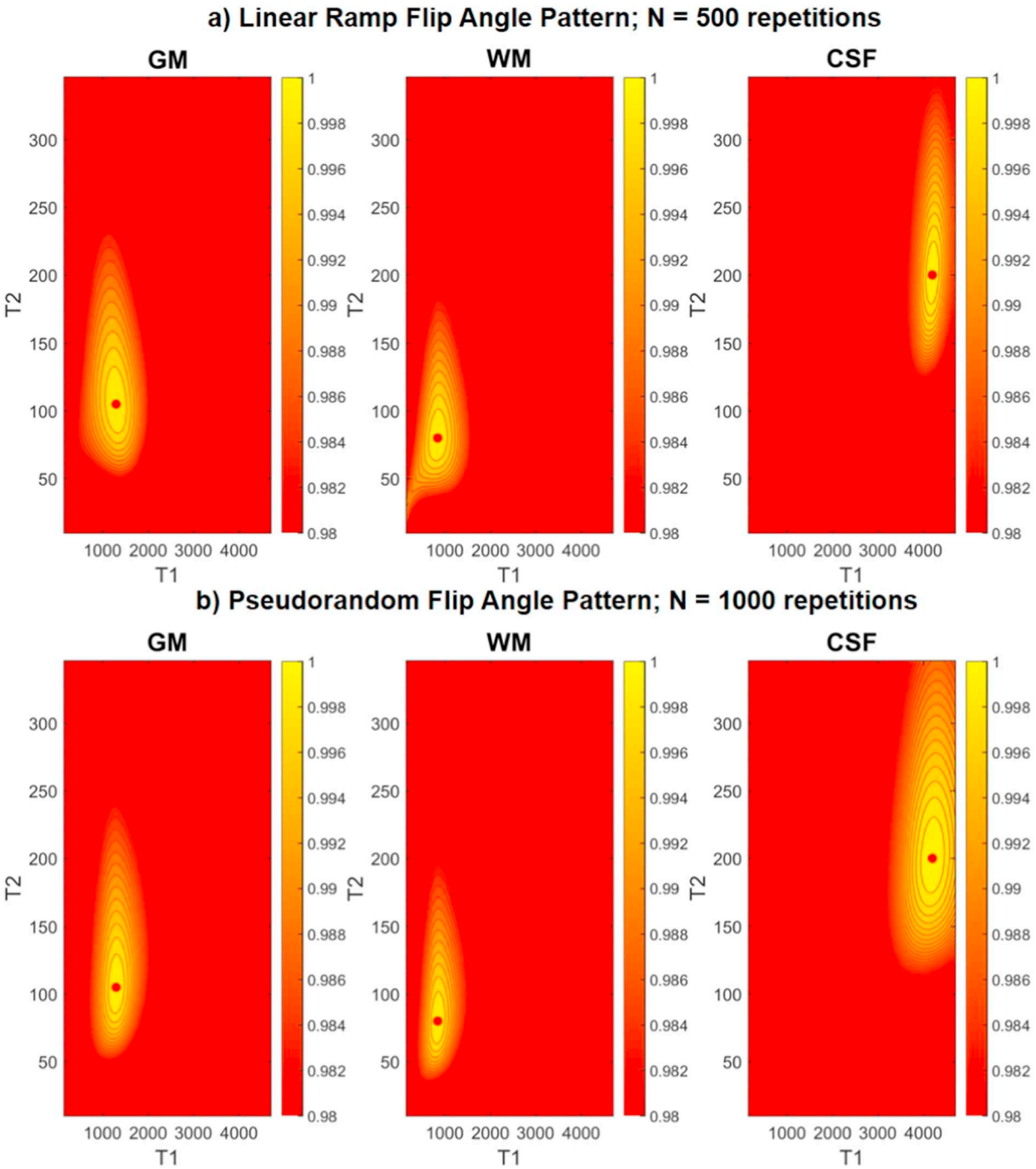

Fig. 1. T1-T2 sensitivity of exemplary values of grey matter (GM; T1 = 1300 ms, T2 = 105 ms), white matter (WM; T1 = 850 ms, T2 = 80 ms) and cerebrospinal fluid (CSF; T1 = 4200 ms, T2 = 200 ms) at 3 T that were simulated for the unbalanced SSFP sequence using the EPG model for (a) Linear Ramp FA Pattern from 1° to 70° with N = 500 repetitions and (b) Pseudorandom FA pattern with N = 1000 repetitions that was used by Jiang et al. [18]. The sensitivity measures the similarity between different T1-T2 responses and hence specifies the accuracy with which a query T1-T2 pair can be matched to the correct dictionary entry in the presence of noise. The tighter the contours, the smaller the range of T1 and T2 valued dictionary atoms to which the query is likely to be matched. Note that both sensitivity plots have the same contour levels for direct comparison between the two FA schedules.

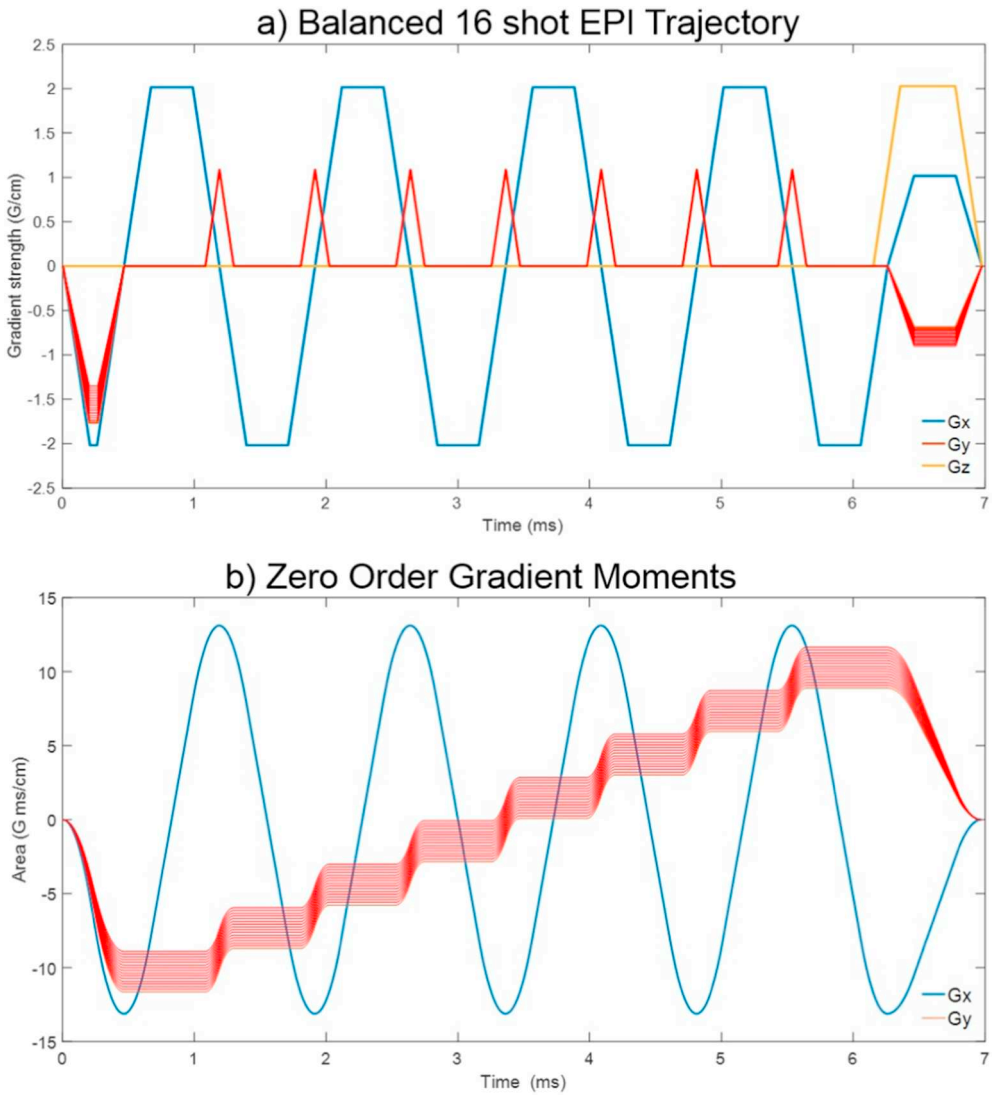

Fig. 2. (a) The 16 shot EPI trajectory showing G_x, G_y, and G_z gradients. Note that the G_y gradients are slightly different for each of the 16 shots indicating that different lines of k_y-space are acquired at every shot. The spoiler gradient G_z dephases the transverse magnetization for every TR making the sequence unbalanced [18]. (b) The corresponding x and y zero order gradient moments for G_x and G_y were nulled to ensure constant residual magnetization for each shot throughout the acquisition.

128 × 128, FOV of 22.5 cm, and a slice thickness of 5 mm. The scan time for each TI experiment was 12.8 min and the total scan time for the entire gold standard T1 experiment was 409.6 min. To calculate T1 values, pixel-based nonlinear least-squares curve fitting was used to fit the magnitude of the IR-SE images to

$$M_z(TI) = M_0\left(1 - e^{\frac{-TI}{T1}}\right)$$

where M_0 is the magnetization at thermal equilibrium, M_z is the longitudinal magnetization that depends on the Inversion Time (TI) and T1 relaxation time of the IR-SE experiment.

The T2 values were measured by multiple single echo spin echo experiments with 12 echo times ranging from 0.02 s to 1 s, parallel imaging ASSET factor 2, TR of 12 s, a matrix size of 128 × 128, FOV of 22.5 cm, and a slice thickness of 5 mm. The scan time for each SE experiment was 12.8 min and the total scan time for the entire gold standard T2 experiment was 153.6 min. To calculate T2 values, the magnitude values from the multiple single echo spin echo images were fit to

$$M_{xy}(TE) = M_0\, e^{\frac{-TE}{T2}}$$

where M_0 is the magnetization at thermal equilibrium, M_{xy} is the transverse magnetization that depends on the Echo Time (TE) and T2 relaxation time of the SE experiment.

2.4. Healthy volunteer brain scans

16-shot EPI-MRF and Spiral-MRF datasets were acquired from three healthy volunteer brains using the linear ramp FA schedule from 1° to 70° for 500 repetitions. The T1 and T2 values estimated by EPI-MRF and Spiral-MRF methods from healthy volunteer brains were compared with conventional T1 and T2 values previously reported in literature [39] and also to T1 and T2 values estimated by an established Spiral-MRF method with pseudorandom FA variation [18]. WM and GM regions were extracted from the healthy volunteer brain images to calculate the accuracy of T1 and T2 quantification. The segmentation was performed by thresholding using the T1 maps. The overall structures of GM and WM were largely captured by the thresholding process. The Matlab Image Processing Toolbox was used for segmentation.

2.5. Reconstruction

The MRF dictionary of magnetic resonance responses was pre-computed offline using a Matlab implementation of the EPG formalism [37,38]. The EPG model is an efficient computational tool for quantitative simulations of signals [18,21,37] obtained from various MRI pulse sequences and is also widely used for characterizing signal evolutions in sequences used for relaxometry (i.e. characterizing relaxation parameters) [40–42]. This model is used to numerically compute the dictionary for MRF sequences by effectively modelling the pathways that lead to the formation of echoes [21,23,42]. A high resolution dictionary having a total of 23,866 dictionary atoms was used with T1 values ranging from 40 ms to 2 s in steps of 20 ms and 2 s to 6 s in steps of 100 ms. The T2 values ranged from 20 ms to 120 ms in steps of 1 ms, 120 ms to 200 ms in steps of 2 ms and 200 ms to 600 ms in steps of 10 ms. The inner product of each of the dictionary atoms and the measured response for each pixel was first computed and the parametric values of the dictionary atom that had the maximum correlation with the measured response was assigned to each pixel.

The dictionary was computed in approximately 5 min on a typical laptop computer with standard specifications (i.e. Intel Core i7 Processor with 16GB RAM). Fig. 3 illustrates the sensitivity of a subset of the dictionary elements. The T1 sensitivity (16 fingerprints of dictionary elements with varying T1 ranging from 100 ms to 700 ms in steps of 40 ms and constant T2 = 100 ms) and T2 sensitivity (17 fingerprints of dictionary elements with varying T2 ranging from 20 ms to 100 ms in steps of 5 ms and constant T1 = 1000 ms) of the sequence for discriminating dictionary elements using a linear ramp FA variation from 1° to 70° are shown for 500 frames. Fig. 3a shows that the T1 sensitivity is high throughout the acquisition and is enhanced by the initial inversion pulse whereas Fig. 3b shows that the T2 sensitivity occurs mostly at higher flip angles (> 20°). Therefore, higher flip angles are needed for efficient T2 discrimination.

The reconstruction was done entirely in Matlab using the code adapted from the works by Ma et al. [17] and Davies et al. [35,36]. Two classes of reconstruction were considered: an IPA reconstruction that included Singular Value Decomposition (SVD) Compression in the Time Domain [25,43–45]; and Dictionary matching (DM) sometimes called

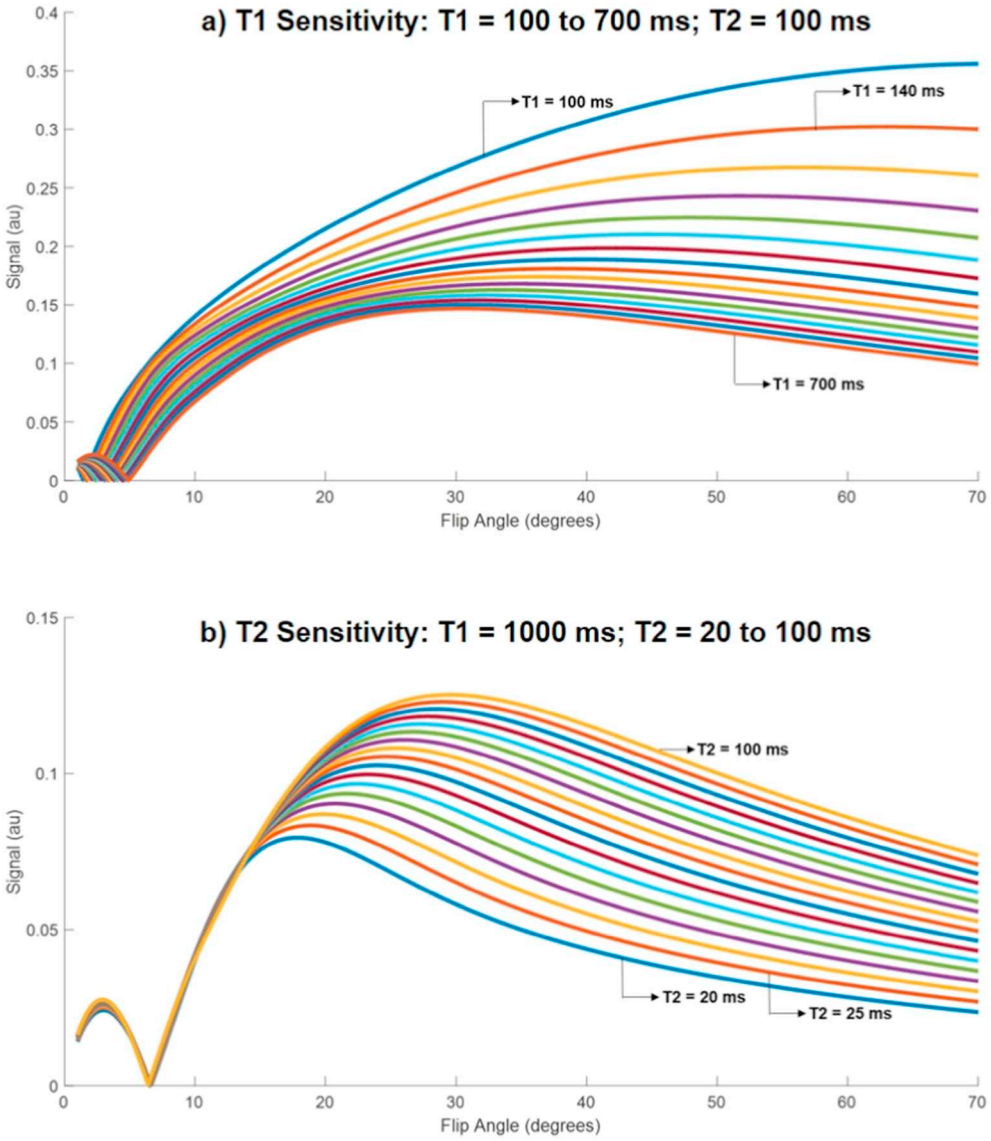

Fig. 3. (a) Figure showing the T1 sensitivity and (b) T2 sensitivity of the sequence for discriminating dictionary atoms when a variable flip angle ramp that linearly varied between 1° to 70° was used during the acquisition for 500 repetitions/frames. The FA for the 1st frame was 1° while the FA for the 500th frame was 70°. Note that the Inversion pulse causes the initial T1 discrimination in (a). These sensitivities were observed at practical T1 and T2 values. Only a subset of the high resolution dictionary is plotted for better visualization. It is also equivalent to label the x-axis in time-points (i.e. seconds). The total acquisition time for a single slice was 8 s.

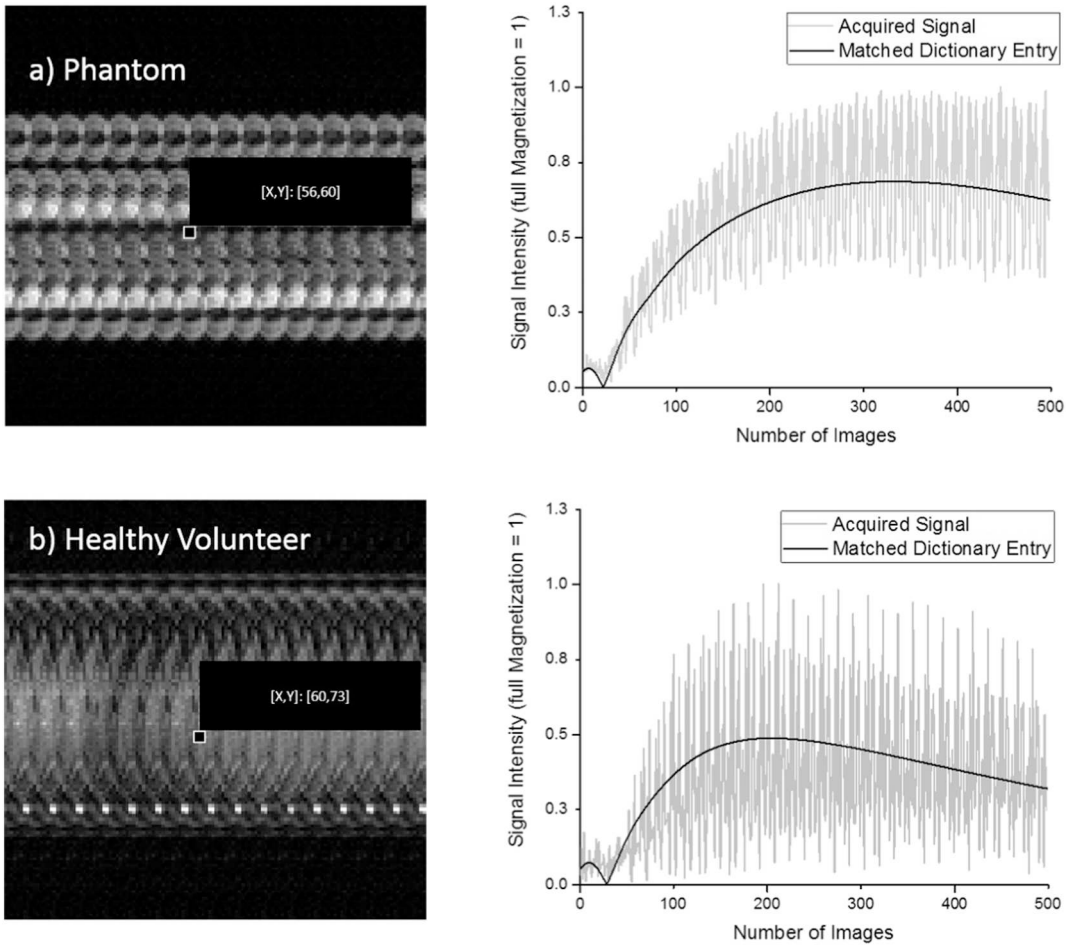

Fig. 4. (a) and (b) show a subsampled zero-filled (ZF) EPI image of phantom and healthy volunteer respectively at a single time-point (t = 1) and the temporal signal curve of one representative voxel over the entire time-series of 500 repetitions together with its corresponding matched dictionary entry. Note that dictionary matching (DM) still works even in the presence of uniform subsampling artefacts in the image due to the noise-like behavior of the signal in the temporal domain.

Matched Filter reconstruction as proposed in the original work on MRF [17], which is equivalent to a single iteration of the IPA reconstruction. The IPA reconstruction is motivated by compressed sensing theory [46–49] and is shown to be capable of removing aliasing artefacts (in the reconstructed images) resulting from severe EPI style k-space subsampling. In the first iteration of IPA, DM was performed on the highly subsampled measurements that were back projected. The back projection included combining multi-coil measurements, a 2D inverse Fast Fourier Transform (FFT) for each temporal slice and a linear temporal compression where the compression bases were pre-calculated using the dominant SVD components of the fingerprint dictionary. The temporal compression was performed primarily to reduce the reconstruction time. The 12 channel multi-coil data was combined coherently using sensitivity maps that were computed from the acquired data [50–52].

Briefly, each iteration of IPA consists of:

$$X^{j+1} = \sigma_D(X^j - \mu A^H(A(X^j) - Y))$$

where $Y \in C^{m \times N}$ are the undersampled k-space measurements across N temporal repetitions and multiple coils, μ is the step size which is adaptively selected through line search [36], $X_j \in C^{n \times N}$ are the spatio-temporal reconstructed images at iteration 'j' and $D \in C^{d \times N}$ denotes the pre-computed dictionary with 'd' atoms (d = 23,866 atoms in this case). The forward and backward operators A, A^H model the multi-coil sensitivities and 2D Fourier Transforms for the acquired subsampled data. The forward and adjoint operators were implemented using the non-uniform fast Fourier Transform (NUFFT) for the spiral reconstruction. Since the spiral readout acquires much denser samples from the centre of k-space than the outer regions, density compensation was performed in both forward and adjoint operations for faster convergence. σ_D denotes the DM step that is used in [25,36] consisting of i) a search over the normalized dictionary atoms to replace the temporal pixels of X^{j+1} with the maximum correlated fingerprints and ii) proton density rescaling.

Therefore, the first iteration of IPA could be interpreted as an application of DM with proton density regularization [35,36]. SVD compression-decompression was also applied iteratively in IPA reconstruction to reduce the complexity of the reconstruction [25,44]. The first 20 dominant singular values were enough to robustly compress the dictionary. The IPA reconstruction was allowed to converge through multiple iterations to improve the data fidelity (i.e. to reduce the relative error between the quantitative estimates of predicted T1 and T2 values and the MRF measurements at each iteration) resulting in more accurate tissue parametric estimations. The convergence occurred when the decrease in relative error between the model fit and acquired measurements did not exceed the specified tolerance level (i.e. 10^{-6}) in successive iterations or if the maximum number of iterations (i.e. 100 in this case) had been reached (whichever occurred sooner).

2.6. Brainweb digital phantom experiment

The Brainweb digital phantom is a realistic, high-resolution, digital, volumetric phantom of the human brain. This three dimensional digital brain phantom defines the spatial distribution for different brain tissues

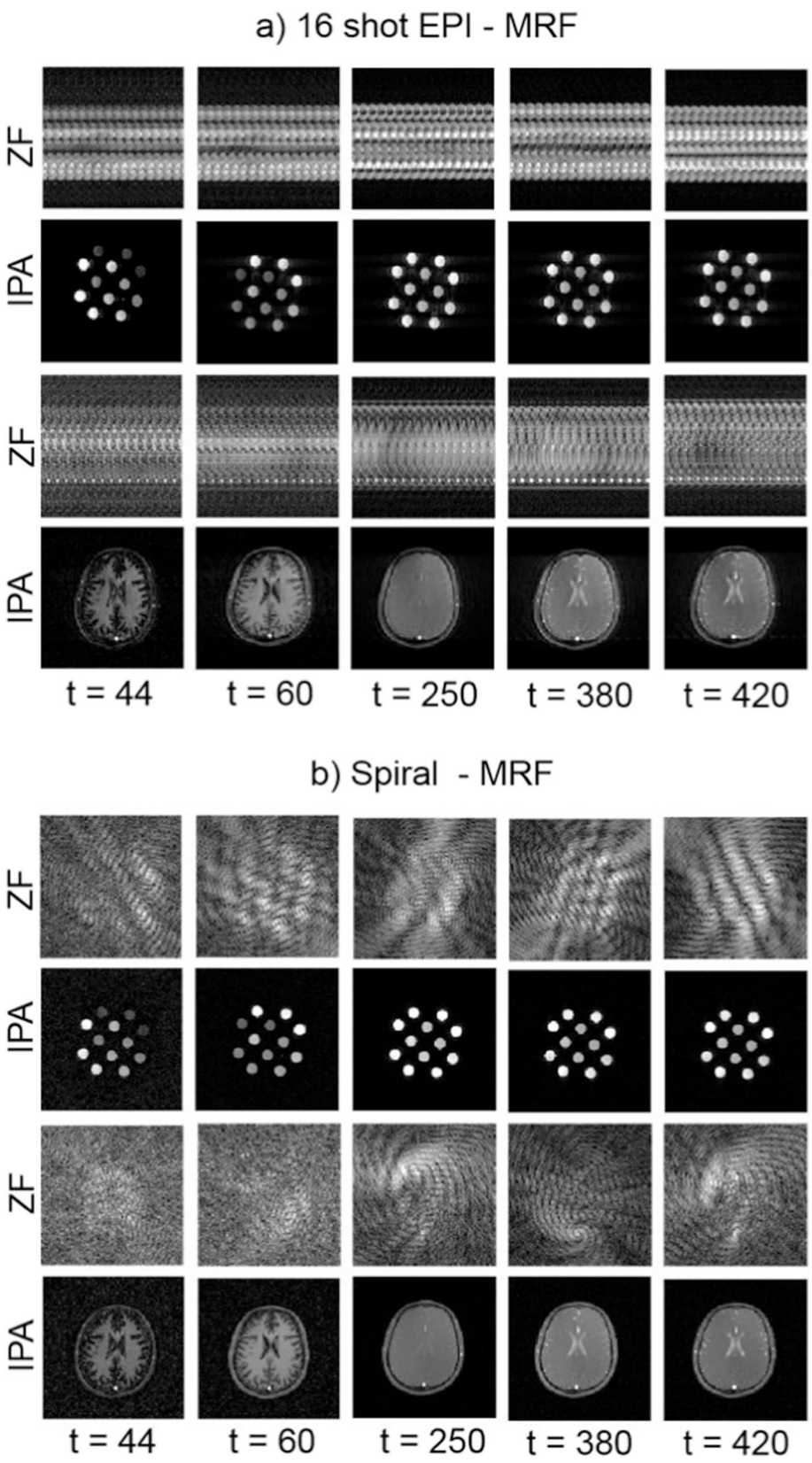

Fig. 5. Figure showing the highly aliased zero-filled (ZF) images and Iterative Projection Algorithm (IPA) reconstructed images at specific time-points (i.e. t = 44, 60, 250, 380, 420) of the tube phantom and the healthy volunteer for (a) EPI-MRF (ramped FA, TR = 16 ms, N = 500 repetitions) and (b) Spiral-MRF (ramped FA, TR = 16 ms, N = 500 repetitions). For DM, the subsampled/aliased ZF images at each frame are used for parameter estimation which is consistent with other work in MRF. However this image sequence should not be considered as an estimate of the actual alias free time series of images. Instead the DM estimates average out the aliasing artefacts. In contrast, for IPA, the subsampled images in each frame are simultaneously reconstructed to produce an alias free time series of images along with parameter estimation.

such as grey matter, white matter, cerebrospinal fluid and muscle, where voxel intensity is proportional to the fraction of tissue within the voxel [53,54]. Since the contribution of each tissue type to each voxel in the brain phantom is known, it can be used as the gold standard to test analysis algorithms such as DM and iterative reconstruction algorithms. The Brainweb digital phantom with known T1 and T2 values, 16-shot EPI subsampling and N = 200 repetitions was used in this study to demonstrate the advantages of iterative reconstruction over non-iterative DM method.

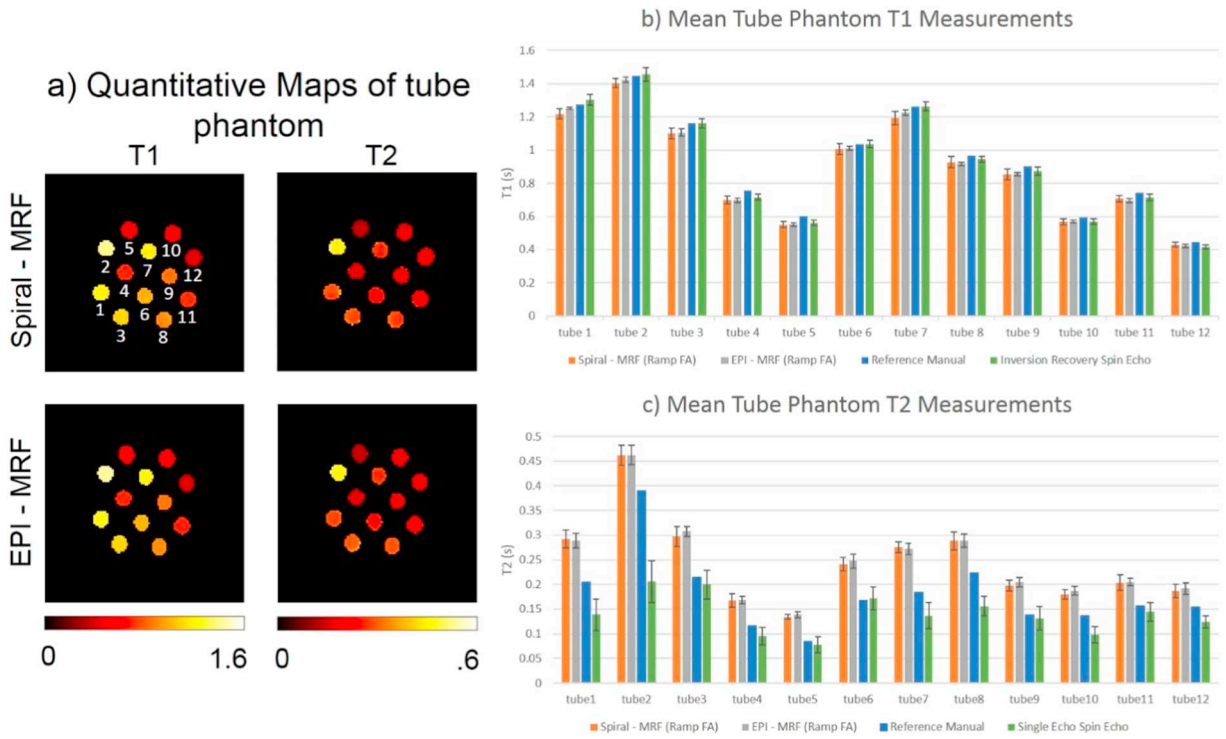

Fig. 6. (a) T1 and T2 maps (in seconds) of the tube phantom generated after Dictionary Matching (DM) for i) Spiral-MRF (ramped FA, TR = 16 ms, N = 500 repetitions) and ii) EPI-MRF (ramped FA, TR = 16 ms, N = 500 repetitions). (b) Mean T1 (± standard deviation) of all tubes in phantom comparing i) Spiral-MRF (ramp FA, TR = 16 ms and N = 500 repetitions) in orange; ii) EPI-MRF (ramp FA, TR = 16 ms and N = 500 repetitions) in grey; iii) reference values from the manufacturer supplied reference document in blue and iv) gold standard measurements in green. (c) Corresponding mean T2 values (± standard deviation). The tubes are numbered in (a) to point out the corresponding tubes in (b) and (c). Note that inversion recovery spin echo (IR-SE) and single echo spin echo (SE) were the gold standard experiments respectively for T1 and T2 estimation. The reference manual supplied by the manufacturer (i.e. Diagnostic Sonar, Livingston, UK) contained reference T1 and T2 values of all the tubes in the phantom. (For interpretation of the references to colour in this figure legend, the reader is referred to the web version of this article.)

3. Results

Fig. 4a and b show a subsampled zero-filled (ZF) EPI image of a phantom and a healthy volunteer respectively at a single time-point (t = 1) and the temporal signal curve of one representative voxel over the entire time-series of 500 repetitions together with its corresponding matched dictionary entry. Although both the phantom and healthy volunteer images are dominated by subsampling artefacts, the DM algorithm is still able to find the corresponding dictionary entry that has the maximum correlation with the acquired data showing its robustness to undersampling artefacts. Note that undersampling artefacts are regular due to uniform subsampling but the signal along the temporal domain is still noise-like which is similar to the Spiral-MRF case as shown by Jiang et al. [18]. This noise-like behaviour of the signal in the temporal domain facilitates effective discrimination between dictionary elements resulting in an accurate dictionary match. Fig. 5 shows the highly aliased zero-filled (ZF) images and Iterative Projection Algorithm (IPA) reconstructed images of the tube phantom and healthy volunteer at specific time-points (i.e. t = 44, 60, 250, 380, 420). It can be seen from the IPA reconstructed images that at lower repetition indexes (i.e. t = 44, 60) the images are predominantly T1 weighted. At higher repetition indexes (i.e. t = 350, 420) the images are more T2-weighted which is in agreement with the parameter encoding (i.e. FA train) used during acquisition. The signal intensity gradually increases due to the linear increase in the flip angles.

Fig. 6a shows the comparison of T1 and T2 maps of i) Spiral- MRF and ii) multi-shot EPI-MRF for the tube phantom which were generated after DM (i.e. single iteration of IPA). The parametric maps are visually comparable for the two methods. Fig. 6b and 6c show the mean (± standard deviation) T1 and T2 values of each tube in the phantom comparing i) Spiral-MRF (ramp FA, TR = 16 ms and N = 500 repetitions) in orange; ii) EPI-MRF (ramp FA, TR = 16 ms and N = 500 repetitions) in grey; iii) reference values from the manufacturer supplied reference document in blue and iv) gold standard measurements in green (i.e. inversion recovery spin echo - IR-SE for T1 estimation and single echo spin echo - SE for T2 estimation). The mean T1 values are in close agreement for all the methods (< 4% variation) while the mean T2 values of Spiral-MRF (in orange) and EPI-MRF (in grey) were similarly close (< 3.5% variation) for all the 12 tubes in the phantom. Fig. 7a shows the generated multi-parametric maps of three healthy volunteer brains after the application of DM for i) Spiral-MRF and ii) EPI-MRF. Detailed structures can be clearly seen in the parametric maps of the healthy volunteer brains in both methods. The mean and standard deviations of WM and GM regions for the cohort of three healthy volunteer brains shown in Fig. 7b and 7c are in agreement with each other for both methods (i.e. < 3% variation for T1 and < 6% variation for T2). These values are also compared with T1 and T2 literature values of an individual healthy volunteer brain that was estimated using an established Spiral-MRF technique with pseudorandom FA, varying TR and N = 1000 repetitions [18] and the gold standard method for conventional T1 and T2 healthy volunteer brain measurements [39].

Fig. 8a shows the original T1, T2 maps of the Brainweb digital phantom [53,54] with corresponding known parameters (T1 s and T2 s) for GM (1.3, 0.105), WM (0.85, 0.08) and CSF (4.2, 0.2) along with the estimated T1 and T2 maps using Dictionary Matching and IPA reconstruction from single-coil Brainweb phantom data. Fig. 8b shows The T1 and T2 difference error maps for Dictionary Matching and IPA reconstruction. Fig. 9 shows the T1 estimations of EPI-MRF for a healthy volunteer brain when IPA was used for reconstruction. Also shown are the T1 maps generated after DM and difference map for

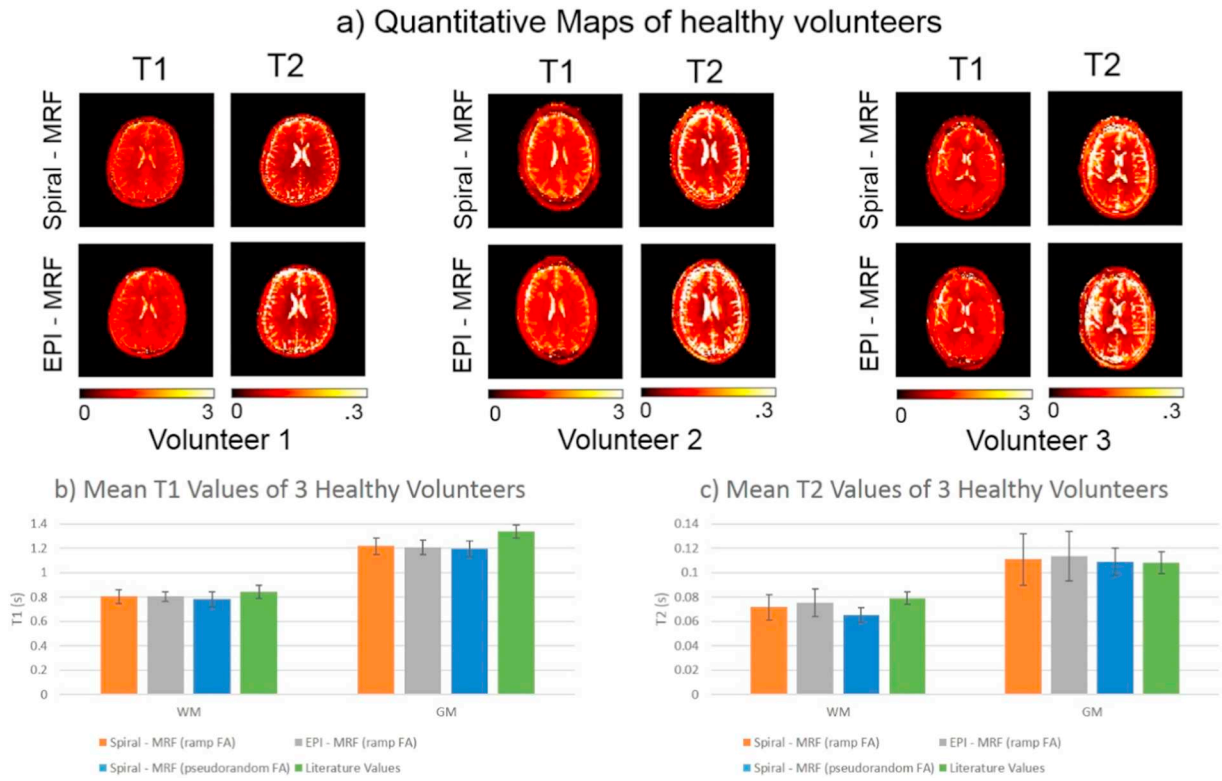

Fig. 7. (a) T1 and T2 maps (in seconds) of three healthy volunteers generated after Dictionary Matching (DM) for i) Spiral-MRF (ramped FA, TR = 16 ms, N = 500 repetitions) and ii) EPI-MRF (ramped FA, TR = 16 ms, N = 500 repetitions). Note the signal loss and signal accrual effects (i.e. susceptibility artefacts) to the left and right of the brain ventricles in the EPI-MRF T2 maps. (b) Mean T1 (± standard deviation) of WM and GM regions of a cohort of three healthy volunteers comparing i) Spiral-MRF (ramp FA, TR = 16 ms and N = 500 repetitions) in orange and ii) EPI-MRF (ramp FA, TR = 16 ms and N = 500 repetitions) in grey. These values are also compared with T1 and T2 literature values of an individual healthy volunteer brain that was estimated using iii) an established Spiral-MRF technique (pseudorandom FA, varying TR and N = 1000 repetitions) in blue [18] and iv) previously reported conventional literature values of a healthy volunteer cohort in green [39]. (c) Corresponding mean T2 values (± standard deviation) for WM and GM regions from three healthy volunteers. (For interpretation of the references to colour in this figure legend, the reader is referred to the web version of this article.)

comparison. The IPA reconstruction reduces the relative error between the quantitative estimates of predicted T1 and T2 values and the MRF measurements at every iteration and converges when this error becomes very small. Fig. 10 shows the corresponding T1 map for Spiral-MRF after IPA reconstruction. In the spiral case, we observe checker board like artefacts (similar to observations reported by Cline et al. [25]) which arise due to lack of samples from the edges of k-space as a result of the spiral sampling strategy. This can be seen as an issue of the null space of the forward operator [25] and is not an algorithmic issue. Iterative reconstructions are particularly beneficial when we have limited data and its benefits are further highlighted in the supplementary material in a reduced coil scenario.

4. Discussion

In this study, a new MRF scheme based on a vastly subsampled Cartesian readout that utilizes multi-shot EPI (i.e. multi-shot EPI-MRF) has been introduced. Good quantification of T1 and T2 maps has been achieved both in phantom and three healthy volunteer brains in about 8 s per slice for the range of T1 and T2 values that normally occur in the human brain. The generated parametric maps of the proposed EPI-MRF method have been compared and are shown to be in good agreement with Spiral-MRF; thereby demonstrating the potential of Cartesian MRF as a suitable alternative to Spiral-MRF. Moreover, EPI sequences have been used clinically for over 20 years and the artefacts that arise from EPI are better understood by clinicians when compared to spirals. Therefore, it has a great potential to be easily adopted in clinical protocols.

On comparison of the T1 and T2 maps of the tube phantom for EPI-MRF and Spiral-MRF in Fig. 6a, it can be seen that both T1 and T2 maps are visually comparable for both methods. The mean T1 and T2 values (see Fig. 6b and 6c) for each of the 12 tubes in the phantom are in close agreement with < 4% deviation for T1 and < 3.5% deviation for T2. The mean T1 values of Spiral-MRF and EPI-MRF were also similarly in very good agreement with the gold standard IR-SE T1 measurements and with the known reference T1 values from the manual (see Fig. 6b). This is due to the high T1 sensitivity of the encoding scheme used for the acquisition resulting in a good T1 quantification. However, despite the good T2 agreement between EPI-MRF and Spiral-MRF for the phantom, we observe that T2 values of the tube phantom overestimate the reference values (see Fig. 6c). In contrast, the gold standard SE measurements appear to slightly underestimate the reference values (and quite considerably in the case of tube 2). The T2 overestimation in MRF may be caused by slice profile and B1 effects which have been previously reported in other MRF studies [21,55–57]. In addition to this, previous MRF studies have reported that T2 variability is greater than T1 in certain gel based phantoms suggesting that T2 is affected more by B1 and temperature fluctuations [19,58]. This T2 discrepancy highlights an inherent limitation of the standard MRF model and not just the proposed methods. This is an important and underreported issue in MRF even though attempts have been made to incorporate correction factors in standard MRF by simulating the radiofrequency pulse in the dictionary, estimating an additional B1 map during the MRF acquisition or by acquiring a B1 field map in a separate scan [21,55]. The main focus of this study is to demonstrate that two different MRF methods (i.e. Spiral-MRF and EPI-MRF) that use the standard MRF model are in agreement with each other for both phantom and healthy volunteer scans. It does not completely account for the

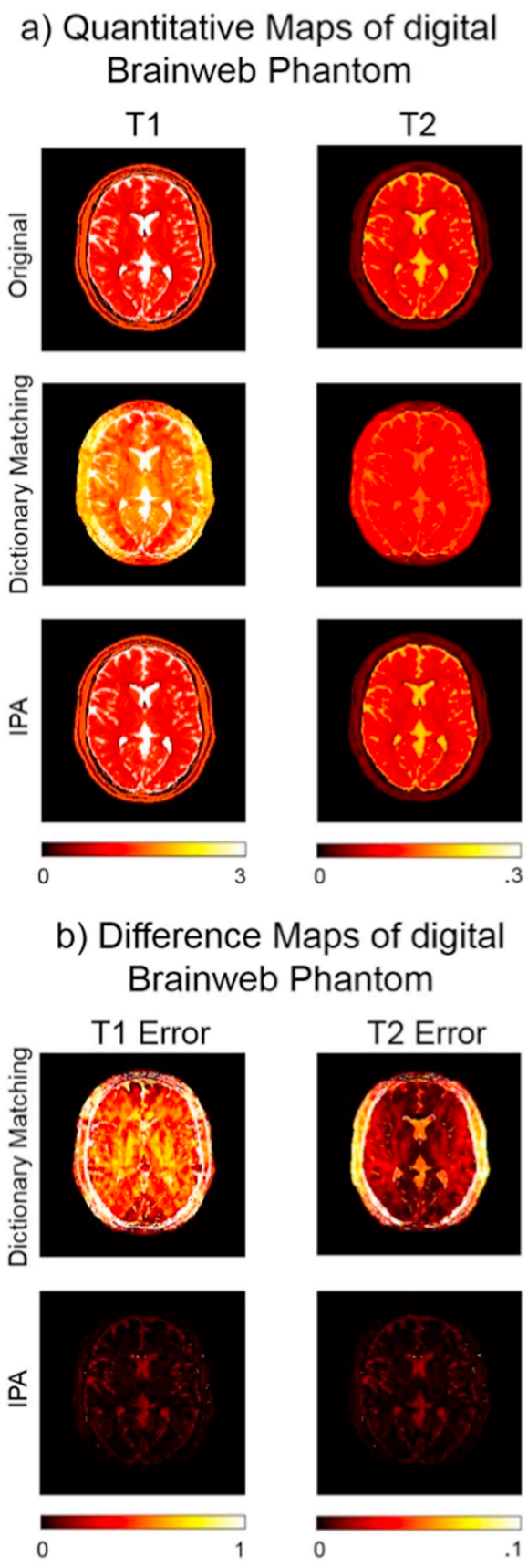

Fig. 8. (a) The original T1,T2 maps of the digital Brainweb Phantom with corresponding known parameters (T1 s and T2 s) for GM (1.3, 0.105), WM (0.85, 0.08) and CSF (4.2 and 0.2) along with the estimated T1 and T2 maps using Dictionary Matching and IPA reconstruction from single-coil Brainweb digital phantom data. (b) The T1 and T2 difference error maps for Dictionary Matching and IPA reconstruction. The maximum T1 and T2 error using DM was 38.09% and 35% respectively whereas the maximum T1 and T2 error using IPA was 3.9% and 5% respectively. The DM method shows poor results since single-coil Brainweb digital phantom data was used to reconstruct the quantitative maps. Aliasing effects are still present inside the brain for DM reconstruction while aliasing is completely resolved when IPA reconstruction is used.

many correction factors necessary to improve the quantitative accuracy of the standard MRF model and is acknowledged as the major disadvantage of this work. Furthermore, it has also been shown in other studies that gold standard T2 measurements are also affected by B1 effects which cause a T2 bias when fitting to the mono-exponential T2 decay curve [59,60]. Additional B1 measurements can also be used to reduce this bias and potentially decrease the discrepancy between MRF and gold standard T2 measurements.

The mean T1 and T2 values of white matter (WM) and grey matter (GM) for three healthy volunteer brains shown in Fig. 7b and 7c for Spiral-MRF and EPI-MRF are almost identical ($< 3\%$ deviation for T1 and $< 6\%$ deviation for T2) and this demonstrates good T1 and T2 quantification for the three healthy volunteer brains. The mean T1 and T2 values of EPI-MRF and Spiral-MRF are also in close agreement with the values obtained by an established Spiral-MRF acquisition with pseudorandom FA schedule, varying TR and $N = 1000$ repetitions [18] and with gold standard T1 and T2 values of healthy volunteers previously reported in the literature [39] (see Fig. 7b and 7c). These results show that the proposed multi-shot Cartesian EPI-MRF approach can be used to generate similar T1 and T2 maps like Spiral-MRF in human brains and can be a good alternative to the Spiral-MRF implementation.

This study also shows the advantages of using iterative reconstruction over the non-iterative DM method. The Brainweb digital phantom [53,54] with known T1 and T2 values, 16-shot EPI subsampling and $N = 200$ repetitions was used to demonstrate the need for iterative reconstruction (see Fig. 8). From the T1 and T2 estimates of DM and IPA reconstructions in Fig. 8a, we can see that a considerable improvement in accuracy was achieved when IPA reconstruction was used. The error maps in Fig. 8b show the reduced error for IPA reconstruction when compared to the DM method. Fig. 9b also shows that there is a reduction in the relative error for EPI-MRF and Spiral-MRF at each iteration until the convergence of the IPA algorithm. The relative error showed an approximate five-fold decrease for EPI-MRF and eight-fold decrease for Spiral-MRF (see Fig. 9b). The IPA reconstructions of multi-shot EPI-MRF converged very quickly (in about 4 iterations) compared to the Spiral-MRF implementation (30 iterations) and could therefore result in a very fast implementation on the scanner. The monotonic decay of the relative error (i.e. measurement fidelity error) implies that iterative reconstructions improved data consistency as compared to the non-iterative DM scheme. Since the entire k-space is sampled in EPI (including high frequency information from the k-space corners), iterative reconstruction improved the T1 estimation and resulted in a very fast convergence especially with the availability of multi-coil data (see Fig. 9a). The DM method shows poor results in Fig. 8 since the Brainweb digital phantom data contains only single coil data. The multi-coil healthy volunteer brain data used in Fig. 9 considerably improves the performance of the DM method since most of the aliasing due to subsampling is removed by using the multiple coils (in a similar way to parallel imaging). While good reconstructions are possible with non-iterative schemes such as DM when multi-coil data is used, iterative methods are beneficial when there is less available data. Here we demonstrated this with a reduced number of coils but it should also be of value when optimizing shorter sequences. In contrast, for the spiral case, due to the lack of sufficient high frequency content, errors

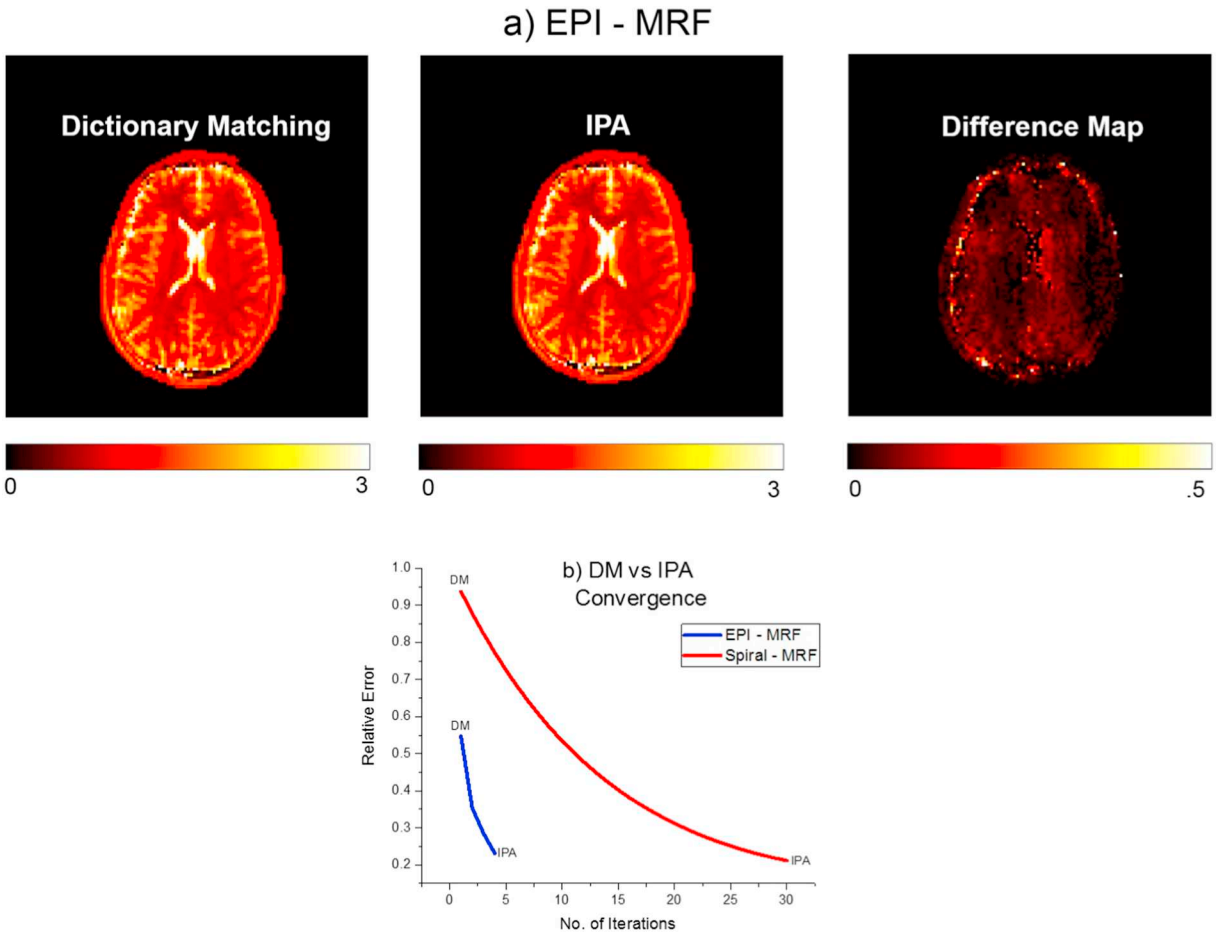

Fig. 9. (a) T1 maps generated using Dictionary Matching (DM) and Iterative Projection Algorithm (IPA) from multi-coil healthy volunteer data along with the difference map for EPI-MRF. (b) A comparison of IPA convergence is shown for EPI-MRF and Spiral-MRF. The multi-coil healthy volunteer brain data considerably improves the performance of the DM method since most of the aliasing inside the brain due to subsampling is removed by using the multiple coils (in a similar way to parallel imaging).

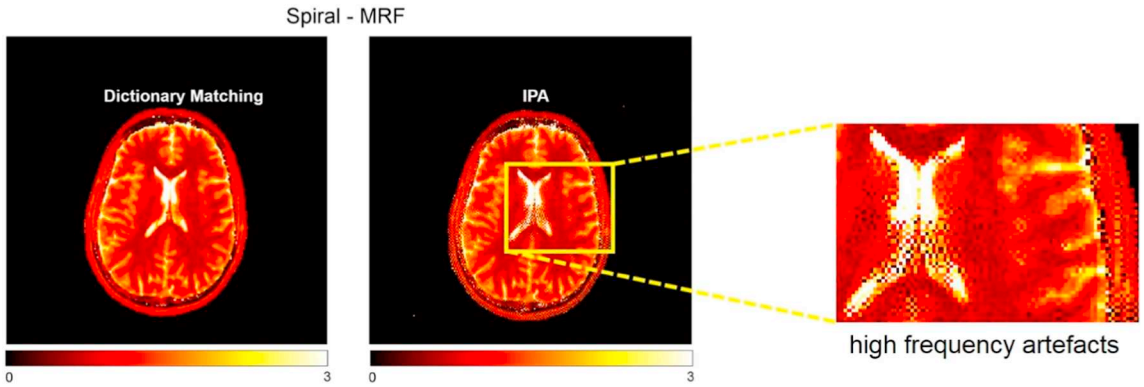

Fig. 10. T1 maps of a healthy volunteer generated using Dictionary Matching (DM) and Iterative Projection Algorithm (IPA) respectively for Spiral-MRF. The enlarged image shows the appearance of high frequency artefacts after iterative reconstruction.

appeared in the iterative reconstruction in the form of checker board like artefacts (similar to the ones reported by Cline et al. [25]) although there was a monotonic decay in the relative error (see Fig. 10). These errors could be removed either by using a spatial-smoothing regularization [61] or by reconstructing images at a lower spatial resolution. These high frequency artefacts coupled with the errors due to re-gridding highlight a fundamental limitation of the spiral sampling strategy [25] which is independent of the algorithm used for reconstruction. Therefore, IPA EPI-MRF may offer a possible route to higher resolution MRF due to its complete k-space coverage [25,62].

The reconstruction times were heavily dependent on the SVD compression-decompression that was used when moving from k-space to image space (i.e. backward or adjoint operation) and vice versa (i.e. forward operation) [25,44]. Each iteration used SVD compression in the backward operation and SVD decompression in the forward operation. This provided a considerable reduction in reconstruction time. The reconstruction time was increased from 22 s to 206 s for EPI-MRF and from 482 s to approximately 6 h for Spiral-MRF when SVD compression-

decompression was not used in the reconstruction. The reconstructions were performed on a normal laptop computer with standard specifications (i.e. Intel Core i7 Processor with 16GB RAM). The convergence of the Spiral- MRF implementation was usually slower (i.e. both in time and in the number of iterations required) when compared to EPIMRF (see Fig. 9b). This appears to be due to the bad conditioning of spiral sampling problem and the need for re-gridding to reconstruct spiral data [25]. In addition, each iteration was more expensive because spiral sampling uses a costlier NUFFT compared to the FFT used in EPI. Therefore, SVD compression-decompression is highly beneficial especially for Spiral-MRF in order to speed up the reconstruction time. Further reductions in the computation time are possible using an adaptive iterative algorithm with fast nearest neighbour searches for the DM step in the reconstruction [62]. The fast convergence of EPI-MRF and its robustness to high frequency artefacts make it naturally suitable for iterative reconstructions.

Despite the enormous potential and numerous advantages of MRF, T1 and T2 quantification through the MRF framework also has some underlying drawbacks that also extend to the proposed EPI-MRF approach. The quantification is not accurate in MRF when T1 and T2 values are very high (i.e. T1 $>$ 2500 ms and T2 $>$ 400 ms) due to the difficulty of discriminating dictionary entries at these values and this can be seen from the underestimation of T2 cerebrospinal fluid (CSF) values in both EPI-MRF and Spiral - MRF in Fig. 7a. In addition, The TR that was used for both EPI and spiral acquisitions was the same. It was set to the minimum achievable TR for EPI (i.e. 16 ms) for fair comparison even though the TR could be further reduced for the case of Spiral-MRF. We have observed in other experiments that there were variations in T2 estimates when different TRs were used (i.e. longer TRs resulting in higher estimates) suggesting that the idealized EPG model used for the dictionary may have some inconsistencies and it merits further research (data not shown). It is also important to note that EPI sequences are more sensitive to B0 inhomogeneity caused by magnetic susceptibility variations that occur in the form of signal loss/leakage in the phase encoding (PE) direction [34,63,64] than spirals. The higher sensitivity of EPI to B0 inhomogeneity is due to its reduced bandwidth in the PE direction. In the human brain, we observe a small signal shift/leakage around the CSF region (i.e. to the left and right of the ventricles in the brain) which is a susceptibility artefact and can be seen from the EPI-MRF T2 maps in Fig. 7a. This is because the CSF has a low susceptibility compared to the iron rich regions surrounding it. However, these local magnetic susceptibility differences are small and do not appear to significantly affect the T2 estimations of GM and WM in human brains as shown by the comparisons in Fig. 7c. Geometric distortions which are common in EPI are also present in the T2 maps in Fig. 7a and might be caused by imperfect phase correction leading to phase errors. It could be reduced by using Echo Time Shifting (ETS) that could be used to improve the phase error function in multi-shot EPI [65]. Due to the high T1 sensitivity of the acquisition, these artefacts were suppressed in the T1 maps but they affected the T2 maps. By enhancing the T2 sensitivity during the acquisition using an optimized FA train, these artefacts could be potentially reduced.

A study of optimized FA schedules is of great interest for our future work which would include finding several optimal parameters that could depend on many factors such as the sequence used (i.e. bSSFP or unbalanced SSFP), excitation sequence length, TRs, the type of variation in flip angles (i.e. smoothly varying, pseudo-random, random, piecewise constant etc.), the amount of subsampling and the type of sampling (i.e. Cartesian, Spiral or Radial). In addition, this future work would include methods to accurately correct for magnetic susceptibility variations, phase errors and also explore high resolution MRF using IPA EPI-MRF. FA schedule optimization, reduction of phase errors and incorporation of correction factors to compensate for T2 quantification errors could potentially improve the robustness of the proposed EPI-MRF method.

5. Conclusion

The multi-shot EPI-MRF method introduced here can provide joint quantification of multi-parametric maps such as T1 and T2 with good accuracy in a short scan duration (i.e. 8s per slice) that is similar to Spiral-MRF. This multi-shot approach not only allows considerable k-space subsampling like spirals but also can achieve a short TR that is comparable to Spiral-MRF. As a result, it can be a suitable alternative for performing MRF using an accelerated Cartesian readout; thereby increasing the potential usability of MRF.

Declaration of Competing Interest

A preliminary version of this work was presented at the Joint Annual Meeting ISMRM-ESMRMB 2018, Paris, June 2018. The authors declare no conflicts of interest.

Acknowledgements

The research leading to these results has received funding from the European Commission H2020 Framework Programme (H2020- MSCA-ITN-2014), number 642685 MacSeNet, the Engineering and Physical Sciences Research Council (EPSRC) platform Compressed Quantitative MRI grant, number EP/M019802/1 and the Scottish Research Partnership in Engineering (SRPe) award, number SRPe PECRE1718/17.

Appendix A. Supplementary data

Supplementary data to this article can be found online at https://doi.org/10.1016/j.mri.2019.04.014.

References

[1] Tofts PS. Chapter 1 - concepts: measurement and MR. Quantitative MRI of the brain: measuring changes caused by disease, Wiley. 2004. p. 3–16.
[2] Warntjes J, Dahlqvist O, Lundberg P. Novel method for rapid, simultaneous T1, T2*, and proton density quantification. Magn Reson Med 2007;57(3):528–37.
[3] Deoni SC. Quantitative relaxometry of the brain. Top Magn Reson Imaging TMRI 2010;21(2):101–13.
[4] Baudrexel S, Nürnberger L, Rüb U, Seifried C, Klein JC, Deller T, et al. Quantitative mapping of T1 and T2* discloses nigral and brainstem pathology in early Parkinson's disease. Neuroimage 2010;51(2):512–20.
[5] Davies G, Hadjiprocopis A, Altmann D, Chard D, Griffin C, Rashid W, et al. Normal appearing grey and white matter t1 abnormality in early relapsing– remitting multiple sclerosis: a longitudinal study. Mult Scler J 2007;13(2):169–77.
[6] Griffin C, Dehmeshki J, Chard D, Parker GJ, Barker G, Thompson A, et al. T1 histograms of normal-appearing brain tissue are abnormal in early relapsing-remitting multiple sclerosis. Mult Scler J 2002;8(3):211–6.
[7] Vrenken H, Geurts JJ, Knol DL, van Dijk LN, Dattola V, Jasperse B, et al. Whole-brain T1 mapping in multiple sclerosis: global changes of normal-appearing gray and white matter. Radiology 2006;240(3):811–20.
[8] Canu E, McLaren DG, Fitzgerald ME, Bendlin BB, Zoccatelli G, Alessandrini F, et al. Mapping the structural brain changes in Alzheimer's disease: the independent contribution of two imaging modalities. J Alzheimers Dis 2011;26(s3):263–74.
[9] Ferreira VM, Piechnik SK, Dall'Armellina E, Karamitsos TD, Francis JM, Choudhury RP, et al. Non-contrast T1-mapping detects acute myocardial edema with high diagnostic accuracy: a comparison to T2-weighted cardiovascular magnetic resonance. J Cardiovasc Magn Reson 2012;14(1):42–53.
[10] Hofer S, Wang X, Roeloffs V, Frahm J. Single-shot T1 mapping of the corpus callosum: a rapid characterization of fiber bundle anatomy. Front Neuroanat 2015;9:1–6.
[11] Knight MJ, McCann B, Tsivos D, Dillon S, Coulthard E, Kauppinen RA. Quantitative T2 mapping of white matter: applications for ageing and cognitive decline. Phys Med Biol 2016;61(15):5587–605.
[12] Verhaert D, Thavendiranathan P, Giri S, Mihai G, Rajagopalan S, Simonetti OP, et al. Direct T2 quantification of myocardial edema in acute ischemic injury. JACC Cardiovasc Imaging 2011;4(3):269–78.
[13] Nishioka H, Nakamura E, Hirose J, Okamoto N, Yamabe S, Mizuta H. Mri T1σ and T2 mapping for the assessment of articular cartilage changes in patients with medial knee osteoarthritis after hemicallotasis osteotomy. Bone Joint Res 2016;5(7):294–300.
[14] Watrin-Pinzano A, Ruaud JP, Cheli Y, Gonord P, Grossin L, Gillet P, et al. T2 mapping: an efficient MR quantitative technique to evaluate spontaneous cartilage repair in rat patella1. Osteoarthr Cartil 2004;12(3):191–200.

[15] Salerno M, Kramer CM. Advances in parametric mapping with CMR imaging. JACC Cardiovasc Imaging 2013;6(7):806–22.
[16] Warntjes J, Leinhard OD, West J, Lundberg P. Rapid magnetic resonance quantification on the brain: optimization for clinical usage. Magn Reson Med 2008;60(2):320–9.
[17] Ma D, Gulani V, Seiberlich N, Liu K, Sunshine JL, Duerk JL, et al. Magnetic resonance fingerprinting. Nature 2013;495(7440):187–92.
[18] Jiang Y, Ma D, Seiberlich N, Gulani V, Griswold MA. MR fingerprinting using fast imaging with steady state precession (FISP) with spiral readout. Magn Reson Med 2015;74(6):1621–31.
[19] Hamilton JI, Jiang Y, Chen Y, Ma D, Lo W-C, Griswold M, et al. MR fingerprinting for rapid quantification of myocardial t1, t2, and proton spin density. Magn Reson Med 2017;77(4):1446–58.
[20] Coppo S, Mehta BB, McGivney D, Ma D, Chen Y, Jiang Y, et al. Overview of magnetic resonance fingerprinting. vol. 65. 2016. p. 12–21.
[21] Buonincontri G, Sawiak SJ. MR Fingerprinting with simultaneous b1 estimation. Magn Reson Med 2016;76(4):1127–35.
[22] Chen Y, Jiang Y, Pahwa S, Ma D, Lu L, Twieg MD, et al. MR fingerprinting for rapid quantitative abdominal imaging. Radiology 2016;279(1):278–86.
[23] Gomez PA, Buonincontri G, Molina-Romero M, Sperl JI, Menzel MI, Menze BH. Accelerated parameter mapping with compressed sensing: an alternative to MR Fingerprinting. Proc Intl Soc Mag Reson Med. 2017. p. 1167.
[24] Hong T, Kim M, Han D, Kim D. Analysis of estimation error from system imperfection in MRF. Proc Intl Soc Mag Reson Med. 2016. p. #437.
[25] Cline CC, Chen X, Mailhe B, Wang Q, Pfeu er J, Nittka M, et al. AIR-MRF: accelerated iterative reconstruction for magnetic resonance fingerprinting. Magn Reson Imaging 2017;41:29–40.
[26] Block KT, Frahm J. Spiral imaging: a critical appraisal. J Magn Reson Imaging 2005;21(6):657–68.
[27] Rieger B, Zimmer F, Zapp J, Weing¨artner S, Schad LR. Magnetic resonance fingerprinting using echo-planar imaging: joint quantification of T1 and T2* relaxation times. Magn Reson Med 2016;78:1724–33.
[28] Cohen O, Sarracanie M, Rosen MS, Ackerman JL. In vivo optimized fast MR fingerprinting in the human brain. Proc Intl Soc Mag Reson med. 2016. p. 430.
[29] Sarracanie M, Cohen O, Rosen MS. 3d balanced-epi magnetic resonance fingerprinting at 6.5 mT. Proc Intl Soc Mag Reson Med. 2015. p. #3385.
[30] Wyatt CR, Grinstead J, Guimaraes A. In vivo T1 and T2 mapping using single-shot EPI fingerprinting. Proc Intl Soc Mag Reson Med. 2017. p. 3895.
[31] Cohen O, Rosen MS. Algorithm comparison for schedule optimization in MR fingerprinting. Magn Reson Imaging 2017;41:15–21.
[32] Bernstein MA, King KF, Zhou XJ. Chapter 16 - echo train pulse sequences. Handbook of MRI pulse sequences. Academic Press; 2004. p. 702–801.
[33] Farzaneh F, Riederer SJ, Pelc NJ. Analysis of T2 limitations and off-resonance effects on spatial resolution and artifacts in echo planar imaging. Magn Reson Med 1990;14(1):123–39.
[34] Hennel F. Multiple-shot echo-planar imaging. Concepts Magn Reson Educ J 1997;9(1):43–58.
[35] M. Davies, G. Puy, P. Vandergheynst, Y. Wiaux, Compressed quantitative MRI: Bloch response recovery through iterated projection, in: Acoustics, speech and signal processing (ICASSP), 2014 IEEE international conference on, IEEE, pp. 6899–6903.
[36] Davies M, Puy G, Vandergheynst P, Wiaux Y. A compressed sensing framework for magnetic resonance fingerprinting. SIAM Journal on Imaging Sciences 2014;7(4):2623–56.
[37] Weigel M, Schwenk S, Kiselev V, Scheffler K, Hennig J. Extended phase graphs with anisotropic diffusion. J Magn Reson 2010;205(2):276–85.
[38] Weigel M. Extended phase graphs: dephasing, RF pulses, and echoes-pure and simple. J Magn Reson Imaging 2015;41(2):266–95.
[39] Wansapura JP, Holland SK, Dunn RS, Ball WS. NMR relaxation times in the human brain at 3.0 tesla. J Magn Reson Imaging 1999;9(4):531–8.
[40] Prasloski T, Mädler B, Xiang Q-S, MacKay A, Jones C. Applications of stimulated echo correction to multicomponent T2 analysis. Magn Reson Med 2012;67(6):1803–14.
[41] Lankford CL, Dortch RD, Does MD. Fast T2 mapping with multiple echo, Caesar cipher acquisition and model-based reconstruction. Magn Reson Med 2015;73(3):1065–74.
[42] Cloos MA, Knoll F, Zhao T, Block KT, Bruno M, Wiggins GC, et al. Multiparametric imaging with heterogeneous radiofrequency fields. Nat Commun 2016;7:1–10.
[43] McGivney DF, Pierre E, Ma D, Jiang Y, Saybasili H, Gulani V, et al. SVD compression for magnetic resonance fingerprinting in the time domain. IEEE Trans Med Imaging 2014;33(12):2311–22.
[44] Assländer J, Cloos MA, Knoll F, Sodickson DK, Hennig J, Lattanzi R. Low rank alternating direction method of multipliers reconstruction for MR Fingerprinting. Magn Reson Med 2018;79(1):83–96.
[45] Zhao B, Setsompop K, Adalsteinsson E, Gagoski B, Ye H, Ma D, et al. Improved magnetic resonance fingerprinting reconstruction with low-rank and subspace modelling. Magn Reson Med 2018;79(2):933–42.
[46] Donoho DL. Compressed sensing. IEEE Trans Inf Theory 2006;52(4):1289–306.
[47] Candes EJ, Romberg JK, Tao T. Stable signal recovery from incomplete and inaccurate measurements. Commun Pure Appl Math 2006;59(8):1207–23.
[48] Lustig M, Donoho D, Pauly JM. Sparse MRI: the application of compressed sensing for rapid MR imaging. Magn Reson Med 2007;58(6):1182–95.
[49] Blumensath T, Davies ME. Iterative hard thresholding for compressed sensing. Appl Comput Harmon Anal 2009;27(3):265–74.
[50] Uecker M, Lai P, Murphy MJ, Virtue P, Elad M, Pauly JM, et al. ESPIRiT - an eigenvalue approach to autocalibrating parallel MRI: where sense meets grappa. Magn Reson Med 2014;71(3):990–1001.
[51] Otazo R, Kim D, Axel L, Sodickson DK. Combination of compressed sensing and parallel imaging for highly accelerated first-pass cardiac perfusion MRI. Magn Reson Med 2010;64(3):767–76.
[52] Pruessmann KP, Weiger M, Scheidegger MB, Boesiger P. SENSE: sensitivity encoding for fast MRI. Magn Reson Med 1999;42(5):952–62.
[53] Collins DL, Zijdenbos AP, Kollokian V, Sled JG, Kabani NJ, Holmes CJ, et al. Design and construction of a realistic digital brain phantom. IEEE Trans Med Imaging 1998;17(3):463–8.
[54] Cocosco CA, Kollokian V, Kwan RK-S, Pike GB, Evans AC. Brainweb: online interface to a 3D MRI simulated brain database. Neuroimage. Citeseer; 1997.
[55] Ma D, Coppo S, Chen Y, McGivney DF, Jiang Y, Pahwa S, et al. Slice profile and b1 corrections in 2D magnetic resonance fingerprinting. Magn Reson Med 2017;78(5):1781–9.
[56] Hong T, Han D, Kim M-O, Kim D-H. RF slice profile effects in magnetic resonance fingerprinting. Magn Reson Imaging 2017;41:73–9.
[57] Chiu SC, Lin TM, Lin JM, Chung HW, Ko CW, Büchert M, et al. Effects of RF pulse profile and intra-voxel phase dispersion on MR Fingerprinting with balanced SSFP readout. Magn Reson Imaging 2017;41:80–6.
[58] Jiang Y, Ma D, Keenan KE, Stupic KF, Gulani V, Griswold MA. Repeatability of magnetic resonance fingerprinting T1 and T2 estimates assessed using the ISMRM/NIST MRI system phantom. Magn Reson Med 2017;78(4):1452–7.
[59] Sled JG, Pike GB. Correction for b1 and b0 variations in quantitative T2 measurements using MRI. Magn Reson Med Off J Int Soc Magn Reson Med 2000;43(4):589–93.
[60] Ben-Eliezer N, Sodickson DK, Block KT. Rapid and accurate T2 mapping from multi spin-echo data using Bloch-simulation-based reconstruction. Magn Reson Med 2015;73(2):809–17.
[61] Beck A, Teboulle M. A fast iterative shrinkage-thresholding algorithm for linear inverse problems. SIAM J Imaging Sci 2009;2(1):183–202.
[62] Golbabaee M, Chen Z, Wiaux Y, Davies ME. Cover tree compressed sensing for fast MR Fingerprint recovery. 2017 IEEE 27th international workshop on machine learning for signal processing (MLSP). 2017. p. 1–6.
[63] Czervionke L, Daniels D, Wehrli F, Mark L, Hendrix L, Strandt J, et al. Magnetic susceptibility artifacts in gradient recalled echo MR imaging. Am J Neuroradiol 1988;9(6):1149–55.
[64] Holland D, Kuperman JM, Dale AM. Efficient correction of inhomogeneous static magnetic field-induced distortion in echo planar imaging. Neuroimage 2010;50(1):175–83.
[65] Feinberg DA, Oshio K. Phase errors in multi-shot echo planar imaging. Magn Reson Med 1994;32(4):535–9.